



Influence of the corona-wire diameter and length on corona discharge characteristics of a cylindrical tri-axial charger



Panich Intra^{a,*}, Artit Yawootti^a, Phadungsak Rattanadecho^b

^a Research Unit of Electrostatic Applications in Energy and Environment (RUÉE), College of Integrated Science and Technology, Rajamangala University of Technology Lanna, Chiang Mai 50220, Thailand

^b Center of Excellence in Electromagnetic Energy Utilization in Engineering (CEEE), Department of Mechanical Engineering, Faculty of Engineering, Thammasat University, Pathum Thani 12121, Thailand

ARTICLE INFO

Article history:

Received 27 July 2014

Received in revised form

10 November 2014

Accepted 20 December 2014

Available online 5 January 2015

Keywords:

Aerosol

Charger

Unipolar charging

Corona discharge

Electric field

ABSTRACT

In this paper, the corona discharge characterization in terms of current–voltage relationships of a unipolar cylindrical tri-axial charger on the effects of the corona wire diameter and length have been experimentally studied and discussed. A commercial computational fluid dynamics software package, COMSOL Multiphysics™, was used to predict the electric field distribution in the ion generation and charging zones of the charger and the ion penetration through the perforated screen opening on the inner electrode of the charger. It was found from experimental results that both positive and negative charging currents in the charging zone of the charger increased with increasing corona and ion-driving voltages. At the same corona and ion-driving voltages, both positive and negative coronas were decreased with increasing diameter of the corona-wire. Compared with the corona-wire of 22 mm in length, the magnitude of both positive and negative charging currents were markedly higher for corona-wire of 11 mm in length at the same corona voltage. It was found that the charging currents for negative coronas were about 1.2 times higher than those positive coronas at the same corona and ion-driving voltages. Numerical results of the electric field distribution and the ion and charged particles migrations in the discharge and charging zones of the charger is correlated to have the same direction with the experimental results of the current–voltage relationships. Also, this can be used to guidance in describing the electric field distribution and the behavior of ion and charged particle trajectories that cannot be seen from experiments in order to improve the applicably design and refinement of a unipolar cylindrical tri-axial charger.

© 2014 Elsevier B.V. All rights reserved.

Introduction

Corona discharge is among the most common technique to produce high ion concentrations in a unipolar field and diffusion charging of aerosol particles in a gas [1]. Electrical aerosol charging by the corona discharges is also common in aerosol size determination by electrical mobility analysis [2]. Corona discharge is usually generated by sharp corners, projecting points, edges of metal surfaces, or small diameter wires at highly curved regions on electrodes. When aerosol flow is directed across the corona discharge and is then charged by attachment of ions produced by the corona discharge. Ions are transported by the electric field and/or by thermal diffusion. Particle charging by transported ions in an

electric field is called “field charging”. For larger particles ($>1 \mu\text{m}$), field charging is dominant. For smaller particles ($<0.1 \mu\text{m}$), thermal diffusion becomes dominant, and “diffusion charging” becomes important [3]. The amount of deposited ion charge on the particle surface depends on resident time, particle radius and shape, electric field, etc.

Electrical aerosol charging by the corona discharge technique has been applied successfully and several designs of aerosol corona charger are employed and described in published literatures for both corona-wire [4–12] and corona-needle chargers [13–19]. In our previous work, Intra [9] was experimentally studied the corona discharge characteristics in a cylindrical tri-axial charger for unipolar diffusion aerosol charging. The ion number concentration in the discharge zone was found larger than that in the charging zone for positive and negative coronas, with values of about 197 and 32 times and 645 and 99 times for the ion-driving voltages of 0 and 310 V, respectively. The average ion penetration for positive and

* Corresponding author.

E-mail address: panich_intra@yahoo.com (P. Intra).

negative coronas was 0.64 and 0.19% and 3.62 and 1.93% for the ion-driving voltages of 0 V and 310 V, respectively. By calculation 14% of charged particles with diameter of 10 nm were lost onto the outer cylinder due to electric field effect. However, the effect of the corona wire diameter and length on the corona discharge within a cylindrical tri-axial charger has not been extensively studied in our previous work and literature. Thus, the influence of the corona wire diameter and length on electrostatic discharge characteristics of a cylindrical tri-axial charger is important for corona discharge due to the presence of different electric field distribution, ion migration and space-charge effect in the ion generation and charging zones of the cylindrical tri-axial charger.

The aim of this paper was to characterize the corona discharge of a unipolar cylindrical tri-axial charger. The experimental results of the corona discharge characterizations in terms of current–voltage relationships of the cylindrical tri-axial charger on the effects of the corona wire diameter and length were studied and discussed. A numerical model is also developed to study the electric field distribution and the ion and charged particle migration behaviors inside this charger that cannot be seen from experiments for a better understanding on the charger operation. This is done by providing predictions of the electric field distribution in the ion generation and charging zones of the charger, the behavior of the ion penetration through the perforated screen opening on the inner electrode of the charger, and also the behavior of the charged particle trajectories in the charging zone of the charger.

Description of cylindrical tri-axial charger

A schematic diagram of the prototype cylindrical tri-axial charger is shown in Fig. 1. The charger's geometrical configuration is similar to that in the unipolar triode charger used by Intra [9]. However, there are differences between those from the triode charger by Intra [9] and the present tri-axial charger, as follows; (i) aerosol flow guide inlet and outlet geometries were modified to ensure uniform flow distribution across the annular entrance to the charging zone in order to reduce diffusion and electrostatic effect losses of the particles inside the charger; (ii) the corona wire electrode in the discharge zone was rearranged to ensure a uniform electric field distribution and stabilize discharge current in order to obtain a high ion concentration in the ion generation zone and a high ion penetration over the perforated screen openings on the inner electrode to the charging zone of the charger; and (iii) it is a

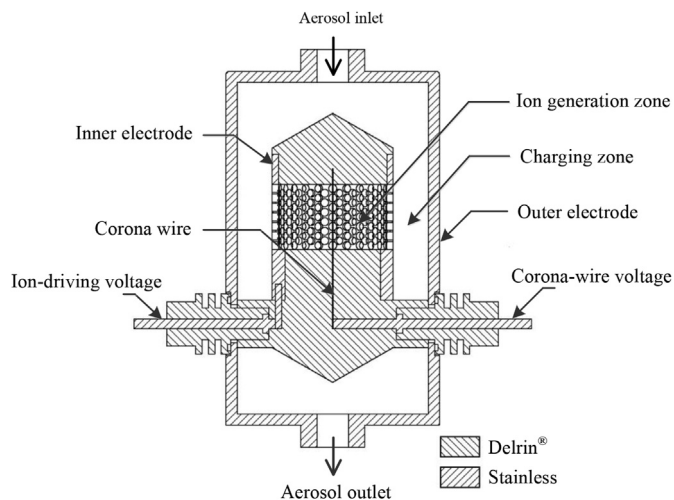


Fig. 1. Schematic diagram of the cylindrical tri-axial charger.

low complexity and inexpensive system. The prototype triode charger was 126 mm in length and 67 mm in diameter.

As Fig. 1 shows, it consisted of two concentric cylinders with a corona-wire electrode placed along the axis of the cylinders. In this study, the corona-wire diameter was set at 0.3, 0.34 and 0.46 mm and length was set at 11 and 22 mm in order to investigate the corona wire diameter and length effects on corona discharge characteristics of the charger as shown in Fig. 2. The inner and outer cylinders were fabricated using stainless steel, and were polished to an extremely fine surface finish to avoid distortion of the electrical field from small surface scratches and imperfections. Stainless steel was used because it is electrically conductive, inert, corrosion resistant and very hard, and therefore resistant to scratching. The inner and the outer radii of the annular charging zone were 17 mm and 30 mm, respectively. The electrical insulation was provided by a Delrin spacer between the inner and outer cylinder, and the aerosol flows through the space between the cylinders. A DC high voltage was applied to the corona-wire to produce a corona discharge and the generated ions is migrated toward the inner cylinder due to the high electric field in the region. In order to allow ions to flow in the charging zone, a section of the inner cylinder was

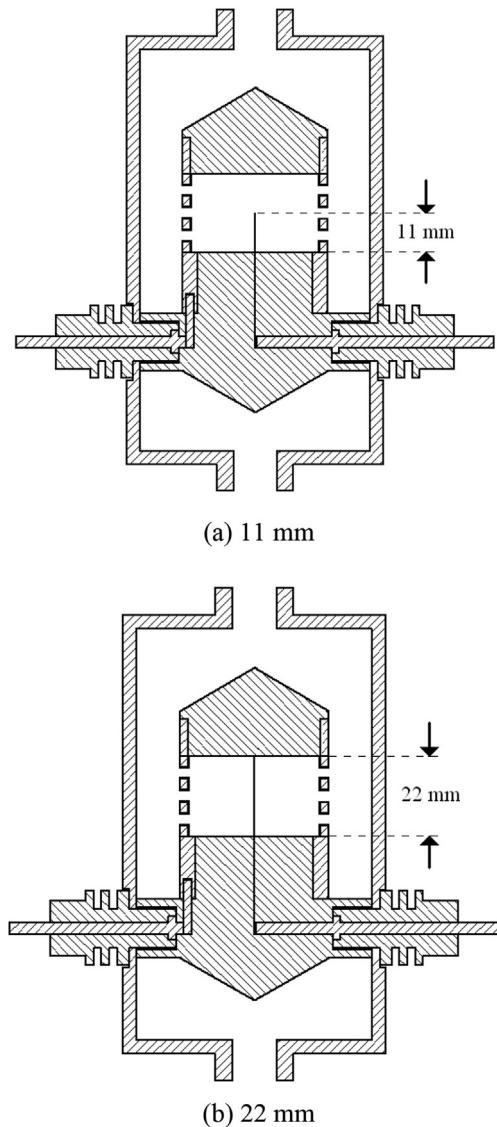


Fig. 2. Arrangements of the corona wire length of the cylindrical tri-axial charger.

made out of a perforated with holes of 2.5 mm in diameter cylindrical tube. The width of the perforated screen opening on the inner cylinder was 20 mm. The ion-driving voltage applied on the inner cylinder forced the ions through the perforated screen openings on the inner cylinder to the charging zone, while the outer cylinder was connected to ground. This ion-driving voltage could regulate the ion current flow through the perforated screen. The fraction of ions drawn into the charging zone is equal to the ratio of the field strengths on either side of the perforated screen opening. In the charging zone, the aerosol particles collided with the ions and were charged electrically.

Ion current density and charging current

The ion current density is the electric current per unit area of cross section (A/m²), and is given by:

$$j = \rho u_{ion} \tag{1}$$

where $\rho = n_{ion}e$, $u_{ion} = Z_{ion}E$, ρ is the space-charge density (C/m³), n_{ion} is the ion concentration (ions/m³), u_{ion} is the ion velocity (m/s), e is the elementary charge (1.60×10^{-19} C), Z_{ion} is the electrical mobility of the ions (m²/V s), and E is the average electric field inside the charging zones of the charger (V/m). Thus, ion current density (A/m²) is given by:

$$j = n_{ion}eZ_{ion}E \tag{2}$$

where $j = i_{ion}/A$, with i_{ion} representing the charging currents and A representing the inner surface area of the outer electrode where the charging current is collected. Thus, the ion current or charging current of the cylindrical tri-axial charger in the absence of aerosol particles can be estimated by:

$$i_{ion} = n_{ion}eZ_{ion}EA \tag{3}$$

Mathematical model and numerical simulation

The important factors influencing on the particle charging efficiency of a corona-based unipolar aerosol charger depending on the arrangement of major geometrical features inside the charger has been well known as the electric field distribution of both ion generation and charging zones, the ion penetration behavior from the ion generation zone through the perforated screen openings on the inner cylinder to the charging zone of the charger, and the charged

particle transport in the charging zone of the charger. As the geometry is very complex, it is difficult to carry out detailed and reliable measurement of the electric field distribution, the ion migration and charged particle trajectories inside this charger from the experimental study. Numerical simulation provides an alternative approach, which is more reliable and less expensive to guidance in describing the electric field distribution and the ion and charged particle migration behaviors inside this charger that cannot be seen from experiments. The mathematical model and numerical simulation used in this study were as follows:

Governing equations

To the accurate model of the ion collector, three partial differential equations (PDE) were selected and coupled in the commercial software package COMSOL Multiphysics™, namely, the Poisson's and Navier–Stokes equations as well as the Khan and Richardson force [20]. The governing equations are given by:

Governing equations for the electrostatics

For electrostatic field modeling of the cylindrical tri-axial charger, electrostatic fields are generated by a combination of stationary charges and applied potentials. Electrostatics is governed by Gauss's Law, which states that the net electric flux passing through a closed surface is equal to the net charge enclosed by that surface. Therefore, the electric potential V is governed by Poisson's equation and given by

$$\nabla^2 V = \frac{\rho_v}{\epsilon_0} \tag{4}$$

where ρ_v is the space charge density and ϵ_0 is the dielectric permittivity of free space. Since most particle charger application involve aerosol concentration lower than 10⁶ particles/cm³, and with low particle charge level, the space-charge effect on the

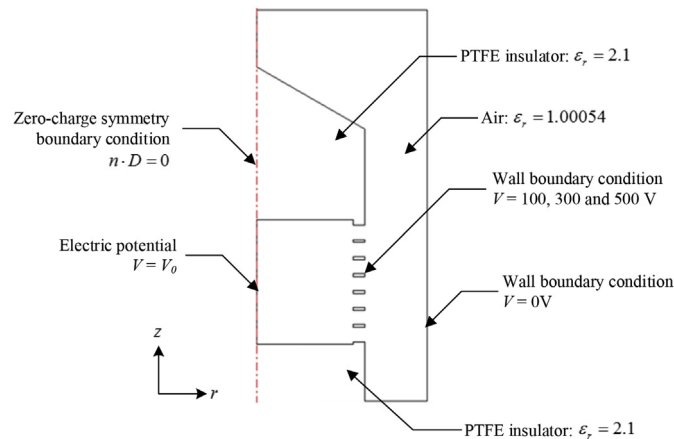


Fig. 3. Computational domain for analysis of electric field inside the cylindrical tri-axial charger.

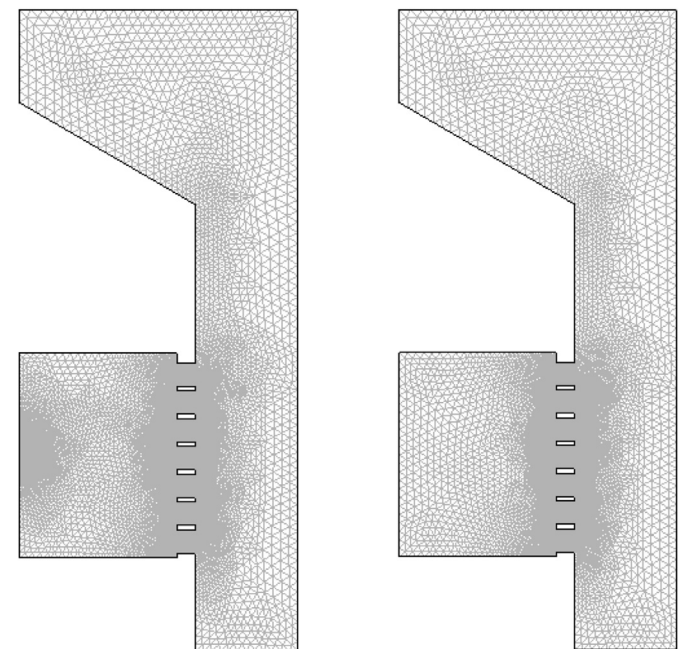


Fig. 4. Mesh distribution for analysis of electric field inside the cylindrical tri-axial charger.

Table 1
Limits of the investigated variables.

Variable	Range
Corona-wire diameter	0.15, 0.17 and 0.23 mm
Corona-wire length	11 and 22 mm
Inner electrode diameter	30 mm
Outer electrode diameter	60 mm
Corona-wire voltage	0–10 kV
Ion-driving voltage	100, 300 and 500 V
Ions generated	Positive ion (+) and negative ion (–)
Ionized gas	Air
Operating pressure	1 atm
Operating temperature	30 °C
Operating humidity	60%

electric field is neglected ($\rho_v = 0$). The electric potential is derived from the electric field intensity E and it is given by

$$E = -\nabla V \quad (5)$$

Governing equations for the air flow

The air flow inside the collector can be assumed to be steady, incompressible and laminar. Based on the principle of momentum conservation, the air flow has been solved by using COMSOL software incorporating a laminar flow, using the Reynolds averaged Navier–Stokes equations for incompressible gas in this work. The mean velocity, field and pressure and determined using the $\kappa - \epsilon$ parameters as defined in the software [20]:

$$\rho_{gas}(u \cdot \nabla)u = -\nabla p + \mu_{gas}\nabla^2 u + F \quad (6)$$

$$\nabla \cdot u = 0 \quad (7)$$

where u is the air velocity, μ_{gas} is the dynamic viscosity of the air, ρ_{gas} is the air density, p is the pressure and F is the force field. The pressure at the outlet is the atmospheric pressure (P_0) and no viscous stress is used:

$$\eta(\nabla u + (\nabla u)^T)n = 0$$

and

$$P = P_0 \quad (8)$$

where T is the transposed matrix. The no slip boundary condition was considered for the wall boundary conditions.

Governing equations for the particle trajectories

There are four forces acting on each charged particle which is given by the gravity force: $\mathbf{F}_g = \rho_p g 2\pi a^3 / 3 \mathbf{z}$, the archimedes force: $\mathbf{F}_a = -\rho_{gas} g 2\pi a^3 / 3 \mathbf{z}$, the electrostatic force: $\mathbf{F}_e = n_p E(r) \cdot \mathbf{r}$ and the drag force: \mathbf{F}_d ; where a is the particle radius, ρ_p is the particle density, n_p is the maximum number of charge per particle, and g is the gravity constant. The drag force is modeled by the Khan and Richardson force which is calculated by the COMSOL software [20]. The following equation describes the total force that a fluid exerts on an immersed spherical particle:

$$\mathbf{F}_d = \pi a^2 \rho_{gas} (\mathbf{u} - \mathbf{u}_p) \left[1.84 (\text{Re}_p)^{-0.31} + 0.293 (\text{Re}_p)^{-0.06} \right]^{3.45} \quad (9)$$

$$\text{Re}_p = \frac{2a\rho_{gas}(\mathbf{u} - \mathbf{u}_p)}{\mu} \quad (10)$$

where Re_p is the particle Reynolds number, \mathbf{u} is the velocity field of the gas and \mathbf{u}_p is the particle velocity.

Computational domain and boundary conditions

Computational domain for analysis of electric field inside the charger is shown in Fig. 3. For the charger, the Poisson's Equation (4) and the electric potential Equation (5) were solved using the electrostatic module and the PDE module to obtain a steady state flow and electric field distributions. Dirichlet boundary conditions were used in the PDE module, with zero space charge density on the corona-wire electrode boundary along with zero ion concentration on the outer electrode. In the electrostatic module, a ground (0 V) has been implemented on the outer electrode. The constant electric potentials were applied to the inner electrode (ranging from 100 to 500 V) as well as the corona-wire electrode (ranging from 0 to 10 kV). The zero-charge symmetry boundary condition was applied to the boundaries without walls, and is given by $n \cdot D = 0$ where n is the outward normal from medium and D is the electric flux density. No heat transfer occurs in the charger could be assumed in this simulation. The flow inside the charger could be assumed to be steady, incompressible and laminar. Based on the principle of momentum conservation, the incompressible Navier–Stokes equations (N–S equation) can be applied in this case. A wall boundary condition has been implemented on both electrodes, i.e., a pressure of 1.01×10^5 Pa on the outlet and a normal velocity field in the inlet. The operating gas was ambient air (density was 1.19 kg/m^3 , viscosity was $1.79 \times 10^{-5} \text{ kg/m/s}$, and the relative permittivity constant was 1.00054). The PTFE insulator permittivity constant was 2.1.

In this study, the charged particle with diameter of $2.5 \mu\text{m}$ and mass of $2.0 \times 10^{-12} \text{ g}$ [21] was used to study behavior of the charged particle trajectories in the charging zone of the charger. The mean of charge per particle was approximated by White's charging equation for the field and diffusion charging [3]. It should be noted that the field charging was dominant for particles larger than $0.5 \mu\text{m}$, and for smaller particles smaller than $0.2 \mu\text{m}$, thermal diffusion became dominant, and therefore diffusion charging became important [21]. In case of the particle diameter of $2.5 \mu\text{m}$, the mean charge per particle were usually based on combined diffusion and field charging where particle charge is the sum of the contributions from field and diffusion charge [22]. Therefore, the mean of charge per particle was about a 1000 electrons for the charged particle with diameter of $2.5 \mu\text{m}$ at the N_{it} product of $2.95 \times 10^{13} \text{ ions/m}^3 \text{ s}$, the corona voltage of 10 kV, the electric field strength of $4.27 \times 10^4 \text{ V/m}$, and the dielectric constant of 3.0, respectively.

Fig. 4 is illustrates the mesh distribution for analysis of the electric field inside the charger. The considered problem was discretized with finite element method (FEM), and utilizing triangular elements for the axis-symmetric two-dimensional model. The mesh was automatically generated by COMSOL [20] and was refined in critical regions such as the inner electrode head and between outer electrode and insulators. This convergence test results in number of triangular elements of approximately 28,960 and 22,368 for corona-wire length of 11 and 22 mm, respectively. The computations were carried out on a desktop running a 64 bit OS Windows 7 Core i5 processors (each 2.40 GHz) and 4 GB of RAM are allowed for solving the model within 5 min of computation time. The values of various parameters, which have been used in this study, are given in Table 1.

Experimental setup

Fig. 5 shows the experimental setup for corona discharge characterization of a cylindrical tri-axial charger. It consisted of a cylindrical tri-axial charger, an adjustable DC high voltage power supply, a Keithley 6517A electrometer, a high efficiency particulate-

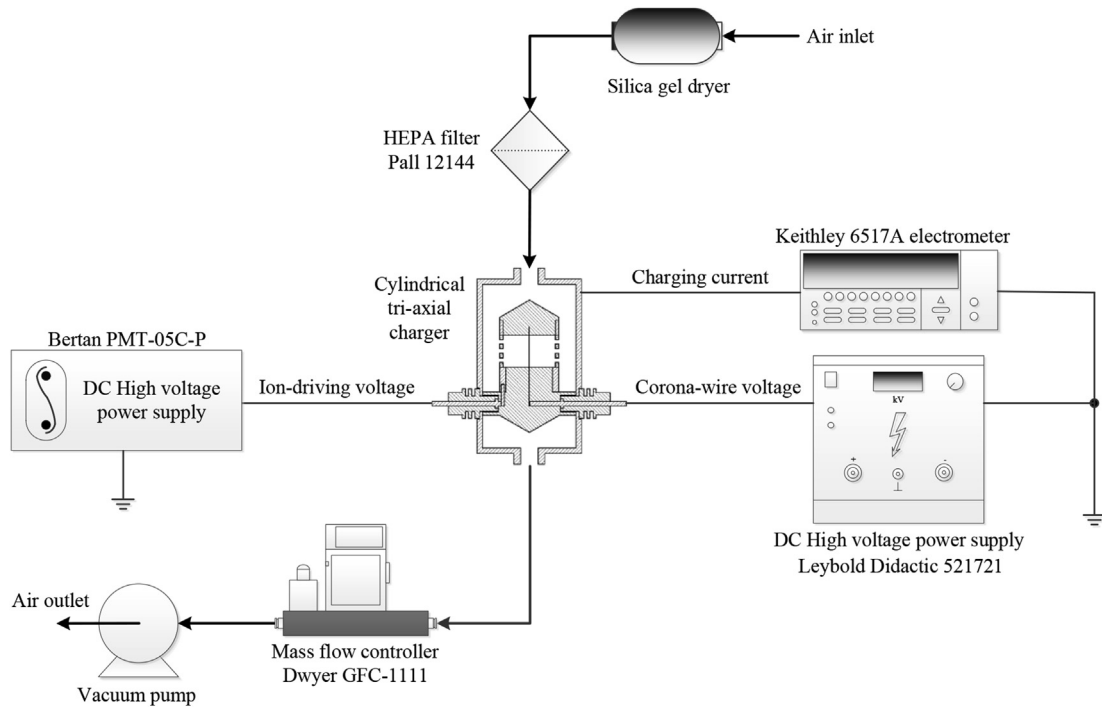


Fig. 5. Experimental setup for electrostatic discharge characterization of a cylindrical tri-axial charger.

free air (HEPA) filter, a Dwyer mass flow controller, and vacuum pump. In order to reduce the space charge and air flow effects in the charging zone, the air flow through the charging zone was regulated and controlled, approximately 5 L/min, by a mass flow meter and controller (Dwyer model GFC-1111) with a vacuum pump located at the end of the experimental equipment train. A diffusion dryer by silica gel drying chamber was used to remove any remaining water from the air sample for stabilize operating humidity, generally is about 60% RH. Dried air samples were filtered through a Pall HEPA capsule filter (model 12144) and were drawn into the charger. The positive and negative high voltage differences on the corona-wire electrode of the charger were applied by a first adjustable commercial DC high voltage power supply (Leybold Didactic model 521721), in the range between 0 and 10 kV. For the ion-driving voltage differences on the inner electrode of the charger, a second adjustable commercial DC high voltage power supply (Bertan model PMT-05C–P) was applied in the range between 100 and 500 V. In order to investigate the ion penetration through the perforated screen opening on the inner electrode into the charging zone of the charger, the charging current from the outer electrode was directly measured by the Keithley 6517A electrometer. It should be noted that the measurements of the charging current was repeated at least three times for each set of operating conditions. Table 1 gives the limits of the evaluated variables.

Results and discussion

The numerical calculation of the vector plot of electric field inside the cylindrical tri-axial charger for the corona-wire length of 11 and 22 mm, the corona-wire voltage of 10 kV and the ion-driving voltage of 100 V, respectively, is shown in Fig. 6. It was shown that non-uniform distribution of electric field appeared at the end of the 11 mm corona-wire in the ion generation zone, on the other hand, a uniform distribution of electric field was observed in the case of 22 mm corona-wire. Fig. 7 shows the numerical results of the

electric field distribution inside the cylindrical tri-axial charger for the corona-wire length of 11 and 22 mm, respectively. In this simulation, the corona-wire voltage was about 10 kV and the ion-driving voltage of 100, 300 and 500 V. The high towards low

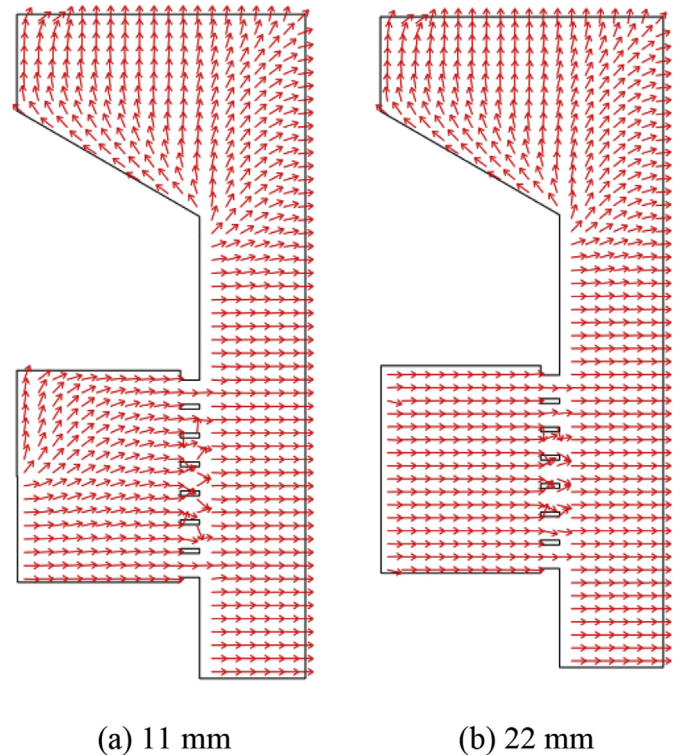


Fig. 6. Numerical calculation of the vector plot of electric field inside the cylindrical tri-axial charger.

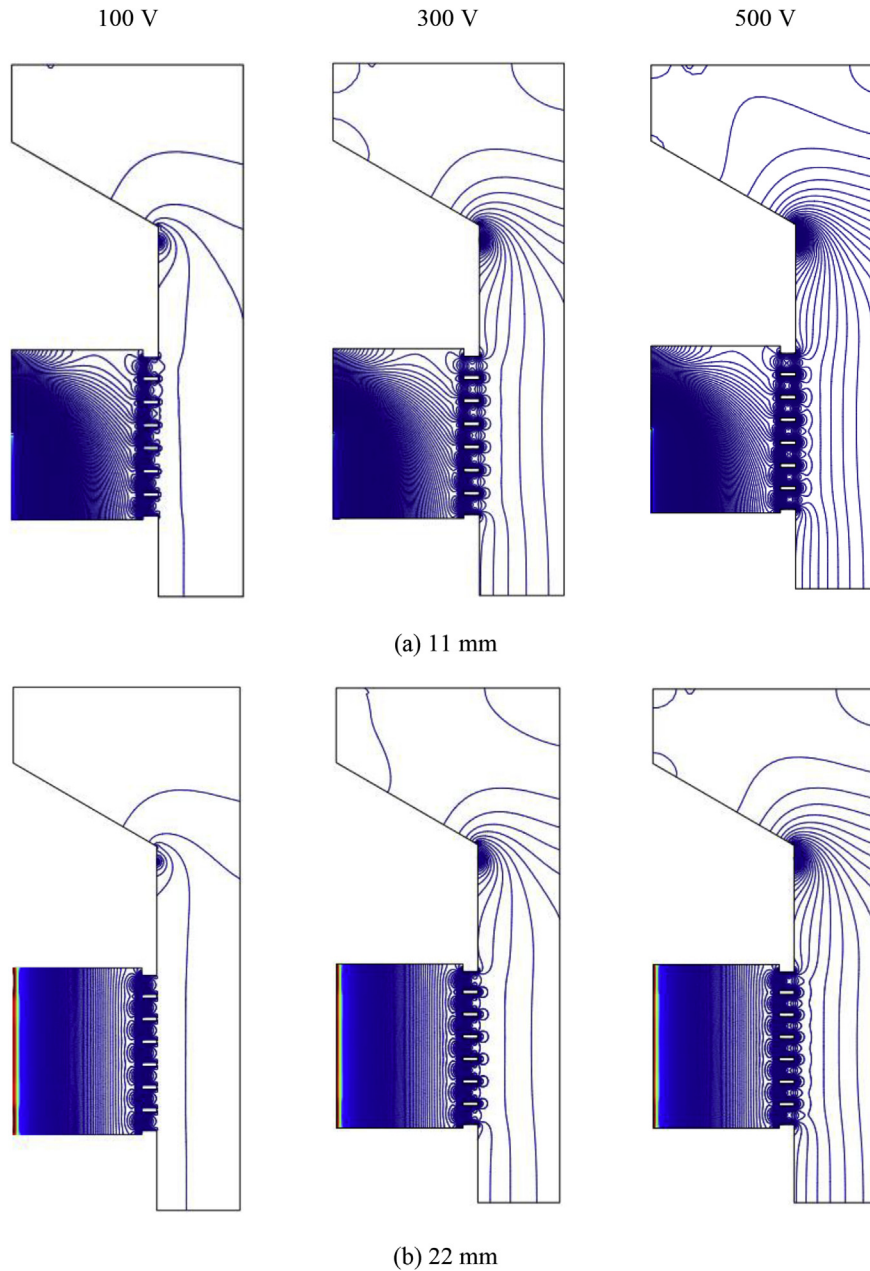


Fig. 7. Numerical calculation of the electric field distribution inside the cylindrical tri-axial charger.

intensity regions are indicated by red (in the web version), yellow, green to blue, respectively. It can be seen that electric field gradients are in orderly manner, as expected. Its gradient was more profound at location near to the corona-wire electrodes for both 11 and 22 mm in length. It should be noted that the corona discharge is generally produced by a non-uniform electrostatic field such as that between a wire/needle and plate or a concentric wire and a tube. Air and other gases can undergo electrical breakdown when the electric field strength is high. For the case of the wire and the tube, the only place this breakdown can occur is in the very thin layer at the wire surface. In this corona region, electrons have sufficient energy to knock an electron from gas molecules to create positive ions and free electrons.

Fig. 8 show the numerical calculation of the electric field flow lines in the ion generation and charging zones of the charger at

corona wire length of 11 and 22 mm, respectively. In this calculation, the corona-wire voltage was fixed at about 10 kV and the ion-driving voltage was about 100, 300 and 500 V. It was noted that the numerical calculation helped predict the electric field flow lines, on which the ions migrated from the ion generation zone into the charging zone within the charger. Therefore, the number of streamlines passing through the perforated screen opening on inner electrode into the charging zone would then be proportional to the ion penetrating from the ion generation zone into the charging zone. As shown in Fig. 8, it was found that the number of electric field flow lines passing through the perforated inner electrode can be increased by increasing the ion-driving voltage into the inner electrode. In the ion generation zone, the non-uniform distribution of the electric field lines was observed at the end of the corona-wire while the 22 mm corona-wire

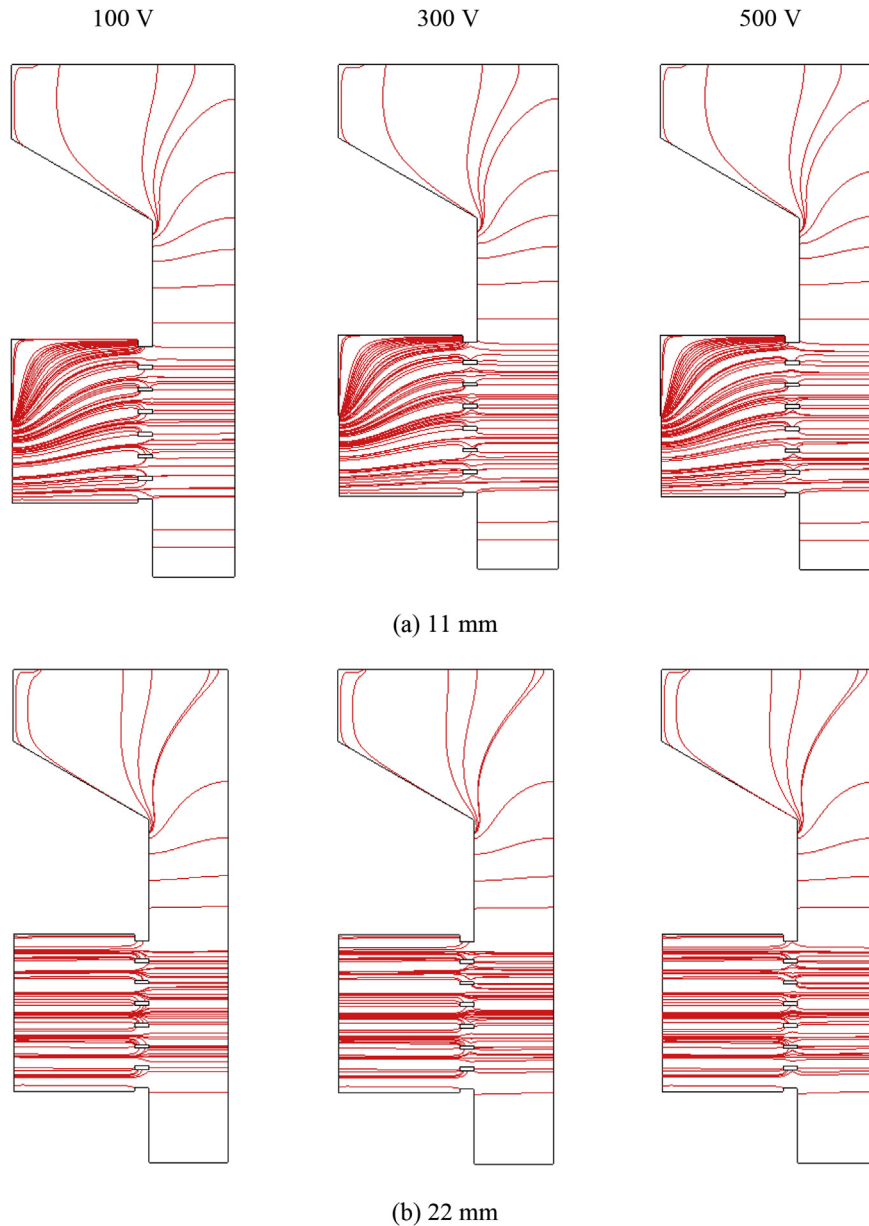


Fig. 8. Numerical calculation of the electric field lines in the ion generation and charging zones of the charger.

appeared to create uniform electric field lines along the radius of the ion generation zone. In the charging zone, it was shown that the number of the electric field lines passing through the perforated screen opening on the inner electrode into the charging zone in the case of 11 mm corona-wire was slightly higher than the case of 22 mm corona-wire. Thus, it can be concluded that the case of 11 mm corona-wire was higher ion penetration corresponding to the ion number concentration in the charging zone of the charger than the case of 22 mm.

In case of particle trajectories, Fig. 9 shows the trajectories of charged particle with diameter of $2.5 \mu\text{m}$ in the charging zone of the charger at different ion-driving voltage of 100, 300 and 500 V with air flow velocity of 0.05 m/s. As shown in Fig. 9, it can be observed that charged particles with diameter of $2.5 \mu\text{m}$ can pass through the charger smoothly without precipitate on the outer electrode of the charger. It was well known that the penetration efficiency of charged particles mainly depended on the electric field

strength in the charging zone of the charger and the particle electrical mobility as a function of a particle diameter. Large particle diameter has higher mean charge than small particle diameter, therefore, electrostatic force applied on the particle increased with respect to the mean charge per particle as a function of its diameter. An increase in electrostatic force on the charged particles produced a decrease in the penetration efficiency of the charged particles in the charging zone of the charger. These calculation results can be used to support the bettering of further modify and refinement of the charger and also to understand the mechanisms of the charged particle transport inside the charger.

The number concentrations of ions in charging zone of the charger can be determined by measuring the charging current because they are approximately proportional. Figs. 10 and 11 show the variations in the charging current in relation with the corona voltage of the charger at different corona wire diameter and length and ion-driving voltage for both positive and negative ions. In this

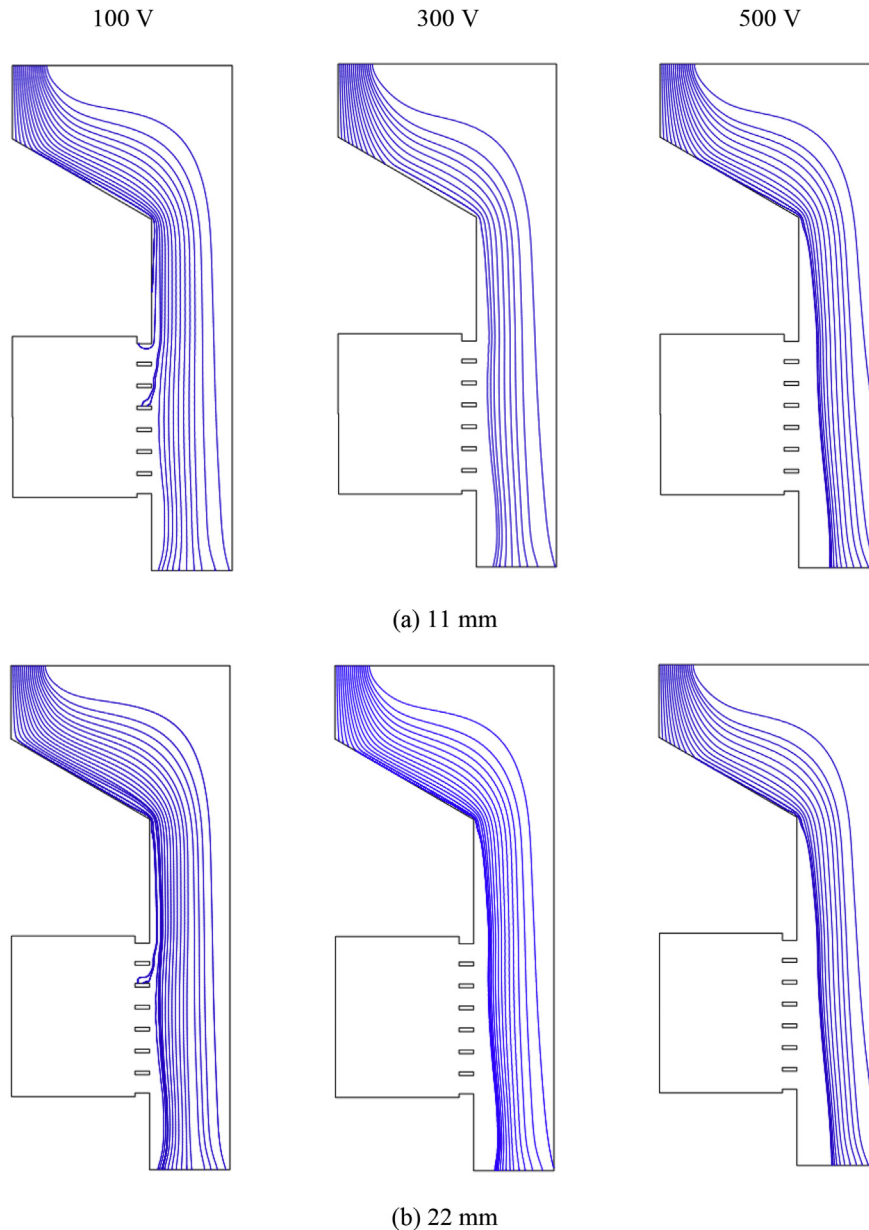
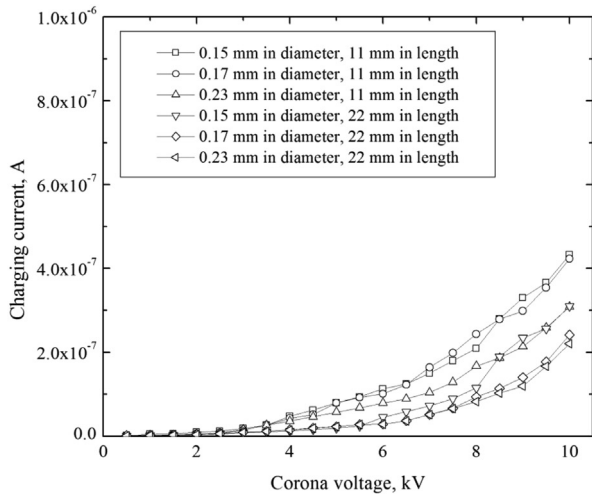


Fig. 9. Numerical calculation of the trajectories of charged particle with diameter of $2.5 \mu\text{m}$ in the charging zone of the charger at different ion-driving voltage.

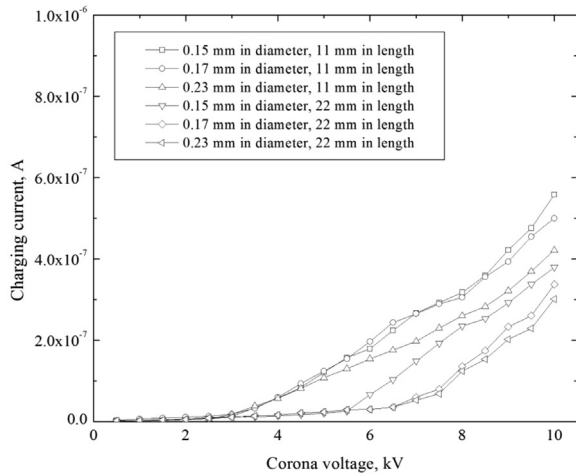
experimentation, the corona voltage was maintained in the range between 0 and 10 kV, the ion-driving voltage was about 100, 300 and 500 V, the corona-wire diameter was about 0.15, 0.17 and 0.23 mm, and the corona-wire length was about 11 and 22 mm. Both positive and negative charging currents increased monotonically with increasing corona voltage at the same ion-driving voltage. When the corona voltage is constant, it was found that the both positive and negative charging currents can be increased by increasing the ion-driving voltage. As shown in Fig. 10, the corona onset voltage in the charging zone of positive corona was about 3.5 kV for the ion-driving voltage of 100, 300 and 500 V, respectively. For negative corona in Fig. 11, the corona onset voltage in the charging zone was about 3.0 kV for ion-driving voltage of 100, 300 and 500 V, respectively. At the same corona and ion-driving voltages, both positive and negative coronas were decreased with increasing corona-wire diameter. This was expected as the corona discharge will occur in a very thin layer at the

corona wire surface corresponding to high strength (potential gradient) of the electric field around the corona-wire in the ion generation zone.

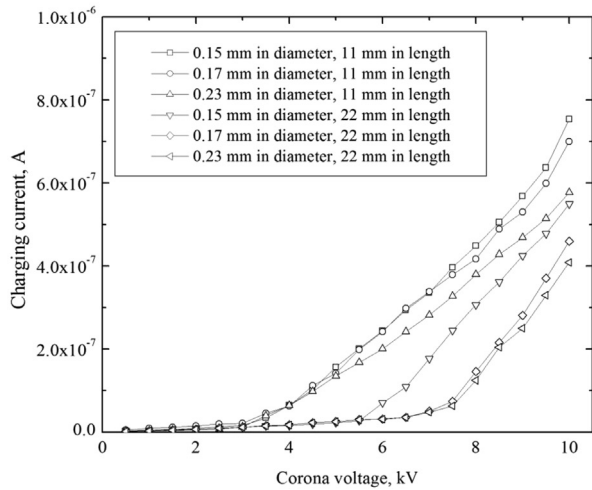
Compared with corona-wire of 22 mm in length, the magnitude of both positive and negative charging currents was markedly higher for corona-wire of 11 mm in length at the same corona voltage because the corona discharge usually forms at highly curved regions on electrodes, such as sharp corners, projecting points, edges of metal surfaces, or small diameter wires. The high curvature causes a high potential gradient at these locations. For positive corona, the highest charging current was found to be about 4.3×10^{-7} , 5.7×10^{-7} and 7.8×10^{-7} A occurring at the corona voltage of 10 kV for the ion-driving voltage of 100, 300 and 500 V, respectively, and corona-wire diameter of 0.15 and length of 11 mm, respectively. For negative corona, the highest charging current was found to be about 5.2×10^{-7} , 7.2×10^{-7} and 9.4×10^{-7} A occurring at the corona voltage of 10 kV for the ion-



(a) 100 V



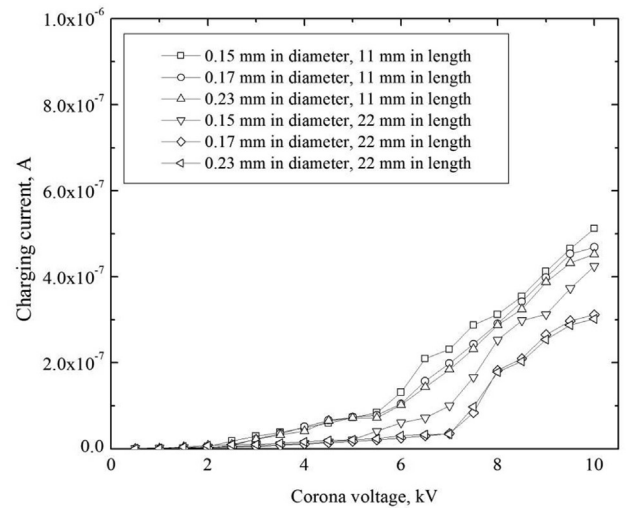
(b) 300 V



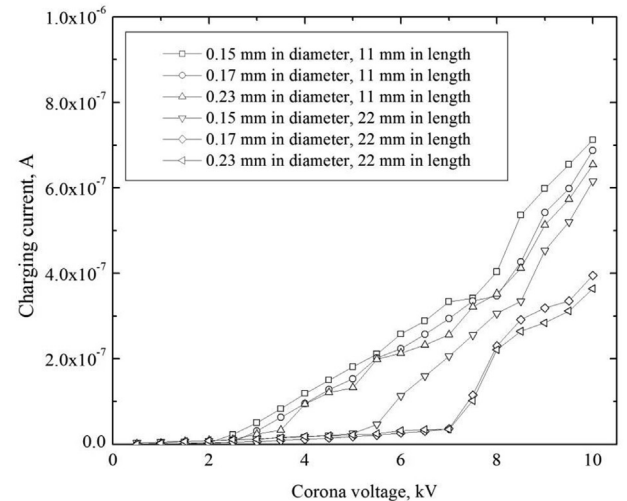
(c) 500 V

Fig. 10. Variations in charging current with corona voltage of the charger at different corona wire diameter and length and ion-driving voltage for positive ion.

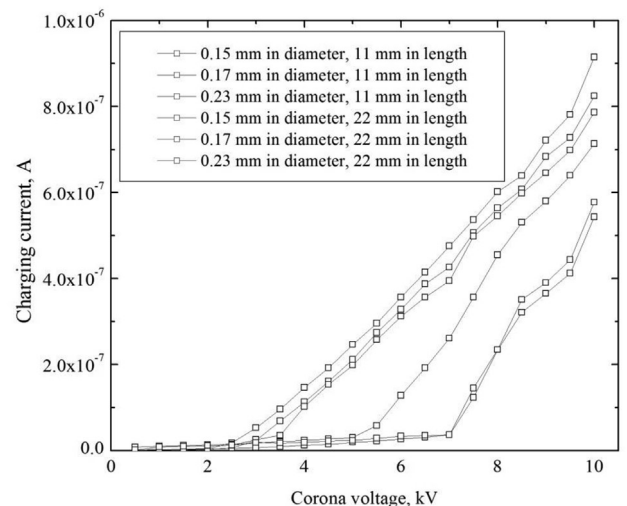
driving voltage of 100, 300 and 500 V, respectively, and corona-wire diameter and length of 0.15 and 11 mm, respectively. At the same corona and ion-driving voltages, the charging currents for negative coronas were about 1.2 times higher than those positive



(a) 100 V



(b) 300 V



(c) 500 V

Fig. 11. Variations in charging current with corona voltage of the charger at different corona wire diameter and length and ion-driving voltage for negative ion.

coronas. This was because negative and positive ions differ in mass and electrical mobility. Ionic mobility was inversely proportional to its mass. Generally, values of mobility for positive and negative ions differ by approximately 19.30%. Reischl et al. [23] quote averages for ion motility as $Z_{ion}^+ = 1.15 \times 10^{-4} \text{ m}^2/\text{V s}$ and $Z_{ion}^- = 1.425 \times 10^{-4} \text{ m}^2/\text{V s}$, respectively.

Conclusion

The effects of the corona wire diameter and length electrostatic discharge characteristics of a unipolar cylindrical tri-axial charger on were numerically and experimentally investigated and presented in this work. A commercial computational fluid dynamics software package, COMSOL Multiphysics™, was used to predict the electrostatic field distribution in the ion generation and charging zones of the charger and the ion penetration through the perforated screen opening on the inner electrode of the charger. In this study, the positively and negatively applied voltages at the corona wire ranged from 0 to 10 kV, the ion-driving voltage between 100 and 500 V, the corona-wire diameter was about 0.15, 0.17 and 0.23 mm, and the corona-wire length was about 11 and 22 mm, respectively. It was found from the experimental results that both positive and negative charging currents in the charging zone of the charger increased with increasing corona and ion-driving voltages. At the same corona and ion-driving voltages, both positive and negative coronas were decreased with increasing corona-wire diameter. Compared with corona-wire of 11 mm in length, the magnitude of both positive and negative charging currents was markedly higher for corona-wire of 22 mm in length at the same corona voltage. It was found that the charging currents for negative coronas were about 1.2 times higher than those positive coronas at the same corona and ion-driving voltages. Numerical calculation results of the electric field distribution and the ion migration in the discharge and charging zones of the charger is correlated to have the same direction with the experimental results of the current–voltage relationships. This can be also used to guidance in describing the electric field distribution and the behavior of ion and charged particle trajectories that cannot be seen from experiments in order to improve the applicably design and refinement of a unipolar cylindrical tri-axial charger.

Acknowledgments

The authors gratefully acknowledge the Thailand Research Fund and the Nation Research University Project of Thailand Office of Higher Education Commission (under the TRF contract No. RTA5680007).

References

- [1] P. Intra, N. Tippayawong, Progress in unipolar corona discharger designs for airborne particle charging: a literature review, *J. Electrostat.* 67 (4) (2009) 605–615.
- [2] P. Intra, N. Tippayawong, An overview of differential mobility analyzers for size classification of nanometer-sized aerosol particles, *Songklanakarin J. Sci. Technol.* 30 (2) (2008) 243–256.
- [3] H.J. White, *Industrial Electrostatic Precipitation*, Addison-Wesley, Reading, Massachusetts, 1963.
- [4] B.Y.H. Liu, K.T. Whitby, H.H.S. Yu, Diffusion charging of aerosol particles at low pressures, *J. Appl. Phys.* 38 (4) (1967) 1592–1597.
- [5] D.Y.H. Pui, *Experimental Study of Diffusion Charging of Aerosols*, Ph.D. thesis, University of Minnesota, Minneapolis, MN, USA, 1976.
- [6] P. Buscher, A. Schmidt-Ott, A. Wiedensohler, Performance of a unipolar “square wave” diffusion charger with variable nt-product, *J. Aerosol Sci.* 25 (4) (1980) 651–663.
- [7] F.E. Kruijs, H. Fissan, Nanoparticle charging in a twin Hewitt charger, *J. Nanopart. Res.* 3 (2001) 39–50.
- [8] B. Biskos, K. Reavell, N. Collings, Electrostatic characterization of corona-wire aerosol charges, *J. Electrostat.* 63 (2005) 69–82.
- [9] P. Intra, Corona discharge in a cylindrical triode charger for unipolar diffusion aerosol charging, *J. Electrostat.* 70 (1) (2012) 136–143.
- [10] C.J. Tsai, G.Y. Lin, H.L. Chen, C.H. Huang, M. Alonso, Enhancement of extrinsic charging efficiency of a nanoparticle charger with multiple discharging wires, *Aerosol Sci. Technol.* 44 (10) (2010) 807–816.
- [11] C.L. Chien, C.J. Tsai, H.L. Chen, G.Y. Lin, J.S. Wu, Modeling and validation of nanoparticle charging efficiency of a single-wire corona unipolar charger, *Aerosol Sci. Technol.* 45 (12) (2011) 1468–1479.
- [12] C.L. Chien, C.J. Tsai, Improvement of the nanoparticle charging efficiency of a single-wire corona unipolar charger by using radial sheath airflow: numerical study, *Aerosol Sci. Technol.* 47 (4) (2013) 417–426.
- [13] K.T. Whitby, Generator for producing high concentration of small ions, *Rev. Sci. Instrum.* 32 (12) (1961) 1351–1355.
- [14] A. Medved, F. Dorman, S.L. Kaufman, A. Pocher, A new corona-based charger for aerosol particles, *J. Aerosol Sci.* 31 (2000) s616–s617.
- [15] A. Hernandez-Sierra, F.J. Alguacil, M. Alonso, Unipolar charging of nanometer aerosol particle in a corona ionizer, *J. Aerosol Sci.* 34 (2003) 733–745.
- [16] M. Alonso, M.I. Martin, F.J. Alguacil, The measurement of charging efficiencies and losses of aerosol nanoparticles in a corona charger, *J. Electrostat.* 64 (2006) 203–214.
- [17] D. Park, M. An, J. Hwang, Development and performance test of a unipolar diffusion charger for real-time measurements of submicron aerosol particles having a log-normal size distribution, *J. Aerosol Sci.* 38 (4) (2007) 420–430.
- [18] P. Intra, N. Tippayawong, Effect of needle cone angle and air flow rate on electrostatic discharge characteristics of a corona-needle ionizer, *J. Electrostat.* 68 (3) (2010) 254–260.
- [19] P. Intra, N. Tippayawong, Design and evaluation of a high concentration, high penetration unipolar corona ionizer for electrostatic discharge and aerosol charging, *J. Electr. Eng. Technol.* 8 (5) (2013) 1175–1181.
- [20] COMSOL Inc., *COMSOL Multi Physics Modelling Guide*, Version 3.5a, 2008.
- [21] W.C. Hinds, *Aerosol Technology*, John Wiley & Sons, New York, USA, 1999.
- [22] B.Y.H. Liu, A. Kapadia, Combined field and diffusion charging of aerosol particles in the continuum regime, *J. Aerosol Sci.* 9 (1978) 227–242.
- [23] G.P. Reischl, J.M. Makela, R. Harch, J. Neced, Bipolar charging of ultrafine particles in the size range below 10 nm, *J. Aerosol Sci.* 27 (6) (1996) 931–939.